11 Phonons and Thermal Properties

James Hone

Department of Physics
University of Pennsylvania
Philadelphia, PA 19104-6317, USA

Abstract. The thermal properties of carbon nanotubes display a wide range of behaviors which are related both to their graphitic nature and their unique structure and size. The specific heat of individual nanotubes should be similar to that of two-dimensional graphene at high temperatures, with the effects of phonon quantization becoming apparent at lower temperatures. Inter-tube coupling in SWNT ropes, and interlayer coupling in MWNTs, should cause their low-temperature specific heat to resemble that of three-dimensional graphite. Experimental data on SWNTs show relatively weak inter-tube coupling, and are in good agreement with theoretical models. The specific heat of MWNTs has not been examined theoretically in detail. Experimental results on MWNTs show a temperature dependent specific heat which is consistent with weak inter-layer coupling, although different measurements show slightly different temperature dependences. The thermal conductivity of both SWNTs and MWNTs should reflect the on-tube phonon structure, regardless of tube-tube coupling. Measurements of the thermal conductivity of bulk samples show graphite-like behavior for MWNTs but quite different behavior for SWNTs, specifically a linear temperature dependence at low T which is consistent with one-dimensional phonons. The room-temperature thermal conductivity of highly-aligned SWNT samples is over 200 W/m-K, and the thermal conductivity of individual nanotubes is likely to be higher still.

1 Specific Heat

Because nanotubes are derived from graphene sheets, we first examine the specific heat C of a single such sheet, and how C changes when many such sheets are combined to form solid graphite. We then in §1.2 consider the specific heat of an isolated nanotube [1], and the effects of bundling tubes into crystalline ropes and multi-walled tubes (§1.3). Theoretical models are then compared to experimental results(§1.4).

1.1 Specific Heat of 2-D Graphene and 3-D Graphite

In general, the specific heat C consists of phonon C_{ph} and electron C_e contributions, but for 3-D graphite, graphene and carbon nanotubes, the dominant contribution to the specific heat comes from the phonons. The phonon contribution is obtained by integrating over the phonon density of states with a convolution factor that reflects the energy and occupation of each phonon state:

$$C_{ph} = \int_0^{\omega_{\max}} k_B \left(\frac{\hbar\omega}{k_B T}\right)^2 \frac{e^{\left(\frac{\hbar\omega}{k_B T}\right)} \rho\left(\omega\right) d\omega}{\left(e^{\frac{\hbar\omega}{k_B T}} - 1\right)^2}, \tag{1}$$

where $\rho(\omega)$ is the phonon density of states and $\omega_{\max}$ is the highest phonon energy of the material. For nonzero temperatures, the convolution factor is 1 at $\omega = 0$, and decreases smoothly to a value of ~ 0.1 at $\hbar\omega = k_B T/6$, so that the specific heat rises with T as more phonon states are occupied. Because $\rho(\omega)$ is in general a complicated function of ω, the specific heat, at least at moderate temperatures, cannot be calculated analytically.

At low temperature ($T \ll \Theta_{\mathrm{D}}$), however, the temperature dependence of the specific heat is in general much simpler. In this regime, the upper bound in Eq. (1) can be taken as infinity, and $\rho(\omega)$ is dominated by acoustic phonon modes, i.e., those with $\omega \to 0$ as $k \to 0$. If we consider a single acoustic mode in d dimensions that obeys a dispersion relation $\omega \propto k^{\alpha}$, then from Eq. (1) it follows that:

$$C_{ph} \propto T^{(d/\alpha)} \qquad (T \ll \Theta_{\mathrm{D}}). \tag{2}$$

Thus the low-temperature specific heat contains information about both the dimensionality of the system and the phonon dispersion.

A single graphene sheet is a 2-D system with three acoustic modes, two having a very high sound velocity and linear dispersion [a longitudinal (LA) mode, with v=24 km/s, and an in-plane transverse (TA) mode, with v=18 km/s] and a third out-of-plane transverse (ZA) mode that is described by a parabolic dispersion relation, $\omega = \delta k^2$, with $\delta \sim 6\times10^{-7}\,\mathrm{m}^2/\mathrm{s}$ [2,3]. From Eq. (2), we see that the specific heat from the in-plane modes should display a T^2 temperature dependence, while that of the out-of plane mode should be linear in T. Equation (1) can be evaluated separately for each mode; the contribution from the ZA mode dominates that of the in-plane modes below room temperature (although the approximation is not valid above 300 K).

The phonon contributions to the specific heat can be compared to the expected electronic specific heat of a graphene layer. The unusual linear k dependence of the electronic structure $E(k)$ of a single graphene sheet at E_F (see Fig. 2 of [4]) produces a low-temperature electronic specific heat that is quadratic in temperature, rather than the linear dependence found for typical metals [5]. Benedict *et al.* [1] show that, for the in-plane modes in a graphene sheet,

$$\frac{C_{ph}}{C_e} \approx (\frac{v_F}{v})^2 \approx 10^4. \tag{3}$$

The specific heat of the out-of plane mode is even higher, and thus phonons dominate the specific heat, even at low T, and all the way to $T = 0$.

Combining weakly interacting graphene sheets in a correlated stacking arrangement to form solid graphite introduces dispersion along the c-axis, as the system becomes three-dimensional. Since the c-axis phonons have very low frequencies, thermal energies of ~50 K are sufficient to occupy all ZA phonon states, so that for $T > 50\,\mathrm{K}$ the specific heat of 3-D graphite is essentially the same as that of 2-D graphene. The crossover between 2-D and interplanar coupled behavior is identified as a maximum in a plot of C_{ph} vs. T^2 [6,7]. We will see below that this type of dimensional crossover also exists in bundles of SWNTs. The electronic specific heat is also significantly changed in going from 2-D graphene to 3-D graphite: bulk graphite has a small but nonzero density of states at the Fermi energy $N(E_F)$ due to c-axis dispersion of the electronic states. Therefore 3-D graphite displays a small linear $C_e(T)$, while C_{ph} has no such term. For 3-D graphite, the phonon contribution remains dominant above ~1 K [8,9].

1.2 Specific Heat of Nanotubes

Figure 1 shows the low-energy phonon dispersion relations for an isolated (10,10) nanotube. Rolling a graphene sheet into a nanotube has two major effects on the phonon dispersion. First, the two-dimensional band-structure of the sheet is collapsed onto one dimension; because of the periodic boundary conditions on the tube, the circumferential wavevector is quantized and discrete 'subbands' develop. From a zone-folding picture, the splitting between the subbands at the Γ point is of order [1]

$$\Delta E = k_{\mathrm{B}} \Theta_{\mathrm{subband}} \approx \frac{\hbar v}{R}, \tag{4}$$

where R is the radius of the nanotube and v is the band velocity of the relevant graphene mode. The second effect of rolling the graphene sheet is to rearrange the low-energy acoustic modes. For the nanotube there are now four,

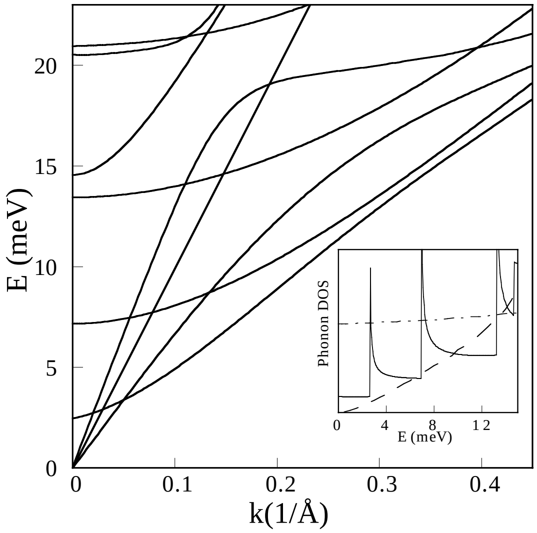

Fig. 1. Low-energy phonon dispersion relations for a (10,10) nanotube. There are four acoustic modes: two degenerate TA modes ($v = 9\,\mathrm{km/s}$), a 'twist' mode ($v = 15\,\mathrm{km/s}$), and one TA mode ($v = 24\,\mathrm{km/s}$) [3]. The inset shows the low-energy phonon density of states of the nanotube (solid line) and that of graphite (dashed line) and graphene (dot-dashed line). The nanotube phonon DOS is constant below 2.5 meV, then increases stepwise as higher subbands enter; there is a 1-D singularity at each subband edge

rather than three, acoustic modes: an LA mode, corresponding to motion of the atoms along the tube axis, two degenerate TA modes, corresponding to atomic displacements perpendicular to the nanotube axis, and a 'twist' mode, corresponding to a torsion of the tube around its axis. The LA mode is exactly analogous to the LA mode in graphene. The TA modes in a SWNT, on the other hand, are a combination of the in-plane and out-of-plane TA modes in graphene, while the twist mode is directly analogous to the in-plane TA mode. These modes all show linear dispersion (there is no nanotube analogue to the ZA mode) and high phonon velocities: $v_{LA} = 24\,\mathrm{km/s}$, $v_{TA} = 9\,\mathrm{km/s}$, and $v_{\mathrm{twist}} = 15\,\mathrm{km/s}$ for a (10,10) tube [3]. Because all of the acoustic modes have a high velocity, the splitting given in Eq. (4) corresponds to quite high temperatures, on the order of 100 K for a 1.4 nm-diameter tube. In the calculated band structure for a (10,10) tube, the lowest subband enters at ~2.5 meV (30 K), somewhat lower in energy than the estimate given by Eq. (4).

The inset to Fig. 1 shows the low-energy phonon density of states $\rho(\omega)$ of a (10,10) nanotube (solid line), with $\rho(\omega)$ of graphene (dot-dashed line) and graphite (dashed line) shown for comparison. In contrast to 2-D graphene and 3-D graphite, which show a smoothly-varying $\rho(\omega)$, the 1-D nanotube has a step-like $\rho(\omega)$, which has 1-D singularities at the subband edges. The markedly different phonon density of states in carbon nanotubes results in measurably different thermal properties at low temperature.

At moderate temperatures, many of the phonon subbands of the nanotube will be occupied, and the specific heat will be similar to that of 2-D graphene. At low temperatures, however, both the quantized phonon structure and the stiffening of the acoustic modes will cause the specific heat of a nanotube to differ from that of graphene. In the low T regime, only the acoustic bands will be populated, and thus the specific heat will be that of a 1-D system with a linear $\omega(k)$. In this limit, $T \ll \hbar v / k_B R$, Eq. (1) can be evaluated analytically, yielding a linear T dependence for the specific heat [1]:

$$C_{ph} = \frac{3k_B^2 T}{\pi \hbar v \rho_m} \times \frac{\pi^2}{3}, \tag{5}$$

where ρ_m is the mass per unit length, v is the acoustic phonon velocity, and R is the nanotube radius. Thus the circumferential quantization of the nanotube phonons should be observable as a linear $C(T)$ dependence at the lowest temperatures, with a transition to a steeper temperature dependence above the thermal energy for the first quantized state.

Turning to the electron contribution, a metallic SWNT is a one-dimensional metal with a non-zero density of states at the Fermi level. The electronic specific heat will be linear in temperature [1]:

$$C_e = \frac{4\pi k_B^2 T}{3\hbar v_F \rho_m}, \tag{6}$$

for $T \ll \hbar v_F / k_B R$, where v_F is the Fermi velocity and ρ_m is again the mass per unit length. The ratio between the phonon and the electron contributions to the specific heat is [1]

$$\frac{C_{ph}}{C_e} \approx \frac{v_F}{v} \approx 10^2, \tag{7}$$

so that even for a metallic SWNT, phonons should dominate the specific heat all the way down to $T = 0$. The electronic specific heat of a semiconducting tube should vanish roughly exponentially as $T \to 0$ [10], and so C_e will be even smaller than that of a metallic tube. However, if such a tube were doped so that the Fermi level lies near a band edge, its electronic specific heat could be significantly enhanced.

1.3 Specific Heat of SWNT ropes and MWNTs

As was mentioned above, stacking graphene sheets into 3-D graphite causes phonon dispersion in the c direction, which significantly reduces the low-T specific heat. A similar effect should occur in both SWNT ropes and MWNTs. In a SWNT rope, phonons will propagate both along individual tubes and

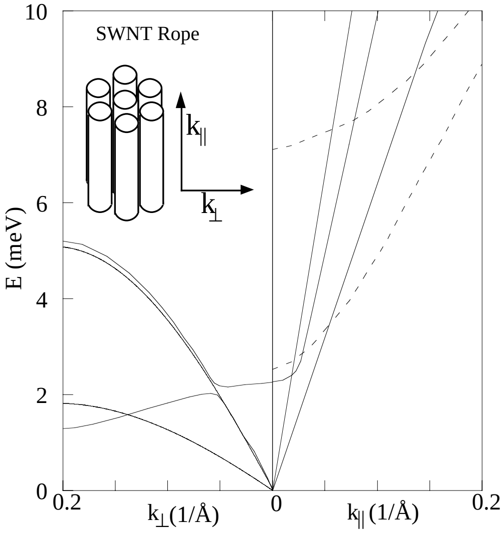

Fig. 2. Calculated dispersion of the acoustic phonon modes in an infinite rope of 1.4-nm diameter SWNTs [6]. The phonon velocity is high in the longitudinal direction and lower in the transverse direction. The first two higher-order subbands (dashed lines) are shown for comparison

between parallel tubes in the hexagonal lattice, leading to dispersion in both the longitudinal (on-tube) and transverse (inter-tube) directions. The solid lines in Fig. 2 show the calculated dispersion of the acoustic phonon modes in an infinite hexagonal lattice of carbon nanotubes with 1.4 nm diameter [6]. The phonon bands disperse steeply along the tube axis and more weakly in the transverse direction. In addition, the 'twist' mode becomes an optical mode because of the presence of a nonzero shear modulus between neighboring tubes. The net effect of this dispersion is a significant reduction in the specific heat at low temperatures compared to an isolated tube (Fig. 3). The dashed lines show the dispersion relations for the higher-order subbands of the tube. In this model, the characteristic energy $k_{\mathrm{B}}\Theta_{\mathrm{D}}^{\perp}$ of the inter-tube modes is ($\sim$ 5 meV), which is larger than the subband splitting energy, so that 3-D dispersion should obscure the effects of phonon quantization. We will address the experimentally-measured inter-tube coupling below.

The phonon dispersion of MWNTs has not yet been addressed theoretically. Strong phonon coupling between the layers of a MWNT should cause roughly graphite-like behavior. However, due to the lack of strict registry between the layers in a MWNT, the interlayer coupling could conceivably be much weaker than in graphite, especially for the twist and LA modes, which do not involve radial motion. The larger size of MWNTs, compared to SWNTs, implies a significantly smaller subband splitting energy [Eq. (4)], so that the thermal effects of phonon quantization should be measurable only well below 1 K.

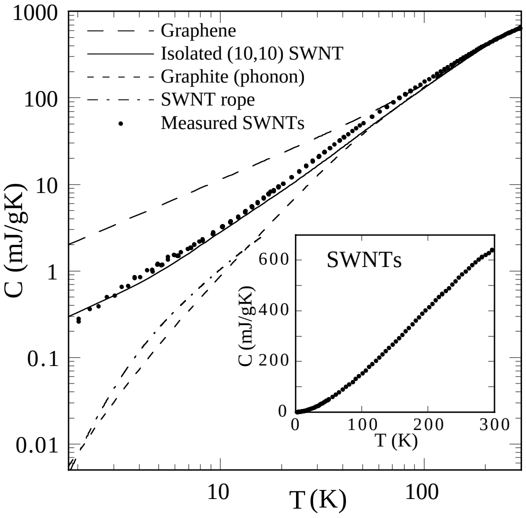

Fig. 3. Measured specific heat of SWNTs, compared to predictions for the specific heat of isolated (10,10) tubes, SWNT ropes, a graphene layer and graphite [11]

1.4 Measured Specific Heat of SWNTs and MWNTs

The various curves in Fig. 3 show the calculated phonon specific heat for isolated (10,10) SWNTs, a SWNT rope crystal, graphene, and graphite. The phonon contribution for a (10,10) SWNT was calculated by computing the phonon density of states using the theoretically derived dispersion curves [3] and then numerically evaluating Eq. 1; $C(T)$ of graphene and graphite was calculated using the model of Al-Jishi and Dresselhaus [12]. Because of the high phonon density of states of a 2-D graphene layer at low energy due to the quadratic ZA mode, 2-D graphene has a high specific heat at low T. The low temperature specific heat for an isolated SWNT is however significantly lower than that for a graphene sheet, reflecting the stiffening of the acoustic modes due to the cylindrical shape of the SWNTs. Below $\sim$ 5 K, the predicted $C(T)$ is due only to the linear acoustic modes, and $C(T)$ is linear in T, a behavior which is characteristic of a 1-D system. In these curves, we can see clearly the effects of the interlayer (in graphite) and inter-tube (in SWNT ropes) dispersion on the specific heat. Below $\sim$50 K, the phonon specific heat of graphite and SWNT ropes is significantly below that of graphene or isolated (10,10) SWNTs. The measured specific heat of graphite [8,9] matches the phonon contribution above 5 K, below which temperature the electronic contribution is also important.

The filled points in Fig. 3 represent the measured specific heat of SWNTs [11]. The measured $C(T)$ agrees well with the predicted curve for individual (10,10) nanotubes. $C(T)$ for the nanotubes is significantly smaller than that of graphene below $\sim$50 K, confirming the relative stiffness of the nanotubes to bending. On the other hand, the measured specific heat is larger than that expected for SWNT ropes. This suggests that the tube-tube coupling in a rope is significantly weaker than theoretical estimates [6,11].

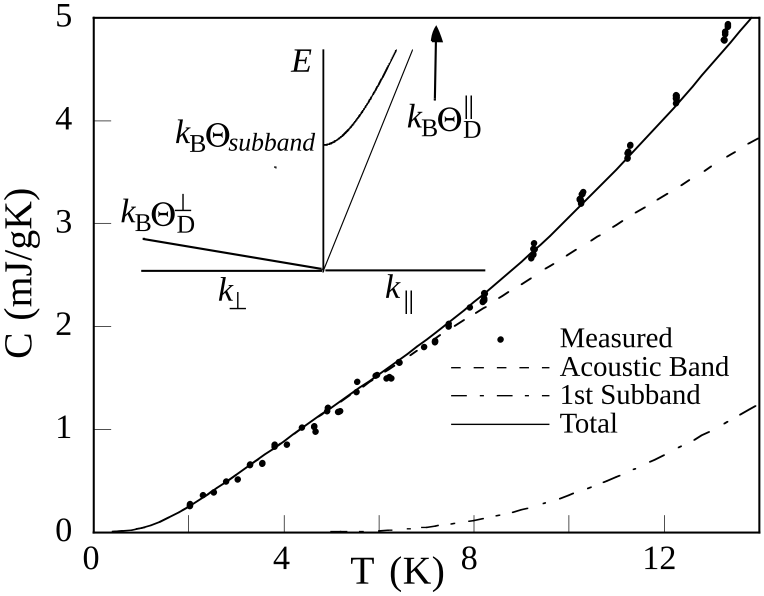

Fig. 4. Measured specific heat of SWNTs compared to a two-band model with transverse dispersion (inset). The fitting parameters used are $\Theta_D^{||} = 960\,\text{K}$; $\Theta_D^{\perp} = 50$ K; and $\Theta_{\text{subband}} = 13\,\text{K}$ [11]

Figure 4 highlights the low-temperature behavior of the specific heat. The experimental data, represented by the filled points, show a linear slope below 8 K, but the slope does not extrapolate to zero at $T = 0$, as would be expected for perfectly isolated SWNTs. This departure from ideal behavior is most likely due to a weak transverse coupling between neighboring tubes. The measured data can be fit using a two-band model, shown in the inset. The dashed line in Fig. 4 represents the contribution from a single (four-fold degenerate) acoustic mode, which has a high on-tube Debye temperature $\Theta_D^{||}$ and a much smaller inter-tube Debye temperature $\Theta_D^{\perp}$. The dot-dashed line represents the contribution from the first (doubly-degenerate) subband, with minimum energy $k_B\Theta_{\text{subband}}$. Because $\Theta_{\text{subband}} > \Theta_D^{\perp}$, the subband is assumed to be essentially one-dimensional. The solid line represents the sum of the two contributions, and fits the data quite well. The derived value for the on-tube Debye temperature is $\Theta_D^{||} = 960\,\text{K}$ (80 meV), which is slightly lower than the value of 1200 K (100 meV) which can be derived from the calculated phonon band structure. The transverse Debye temperature $\Theta_D^{\perp}$ is 13 K (1.1 meV), considerably smaller than the expected value for crystalline

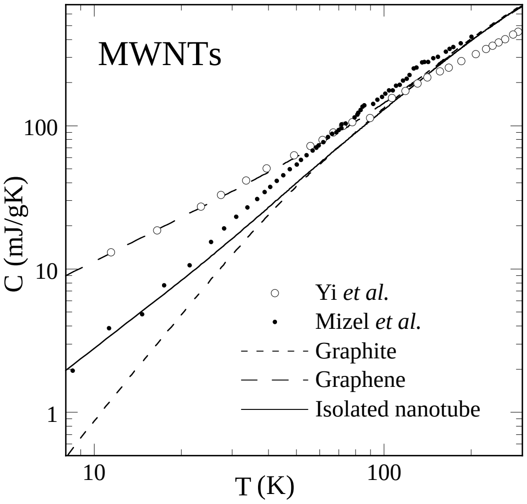

Fig. 5. Measured specific heat of MWNTs [6,13], compared to the calculated phonon specific heat of graphene, graphite, and isolated nanotubes

ropes (5 meV) or graphite (10 meV). Finally, the derived value of $\Theta_{\mathrm{subband}}$ is 50 K (4.3 meV), which is larger than the value of 30 K (2.5 meV) given by the calculated band structure [3].

Figure 5 shows the two reported measurements of the specific heat of MWNTs, along with the theoretical curves for graphene, isolated nanotubes, and graphite. Yi *et al.* [13] used a self-heating technique to measure the specific heat of MWNTs of 20-30 nm diameter produced by a CVD technique, and they find a linear behavior from 10 K to 300 K. This linear behavior agrees well with the calculated specific heat of graphene below 100 K, but is lower than all of the theoretical curves in the 200-300 K range. Agreement with the graphene specific heat, rather than that for graphite, indicates a relatively weak inter-layer coupling in these tubes. Because the specific heat of graphene at low T is dominated by the quadratic ZA mode, the authors postulate that this mode must also be present in their samples. As was discussed above (§1.1,1.2), such a band should should not exist in nanotubes. However, the phonon structure of large-diameter nanotubes, whose properties should approach that of graphene, has not been carefully studied. Mizel *et al.* report a direct measurement of the specific heat of arc-produced MWNTs [6]. The specific heat of their sample follows the theoretical curve for an isolated nanotube, again indicating a weak inter-layer coupling, but shows no evidence of a graphene-like quadratic phonon mode. At present the origin of the discrepancy between the two measurements is unknown, although the sample morphologies may be different.

2 Thermal conductivity

Carbon-based materials (diamond and in-plane graphite) display the highest measured thermal conductivity of any known material at moderate temperatures [14]. In graphite, the thermal conductivity is generally dominated by phonons, and limited by the small crystallite size within a sample. Thus the apparent long-range crystallinity of nanotubes has led to speculation [15] that the longitudinal thermal conductivity of nanotubes could possibly exceed the in-plane thermal conductivity of graphite. Thermal conductivity also provides another tool (besides the specific heat) for probing the interesting low-energy phonon structure of nanotubes. Furthermore, nanotubes, as low-dimensional materials, could have interesting high-temperature properties as well [16]. In this section, we will first discuss the phonon and electronic contributions to the thermal conductivity in graphite. Then we will examine the thermal conductivity of multi-walled and single-walled nanotubes.

The diagonal term of the phonon thermal conductivity tensor can be written as:

$$\kappa_{zz} = \sum C {v_z}^2 \tau, \tag{8}$$

where C, v, and τ are the specific heat, group velocity, and relaxation time of a given phonon state, and the sum is over all phonon states. While the phonon thermal conductivity cannot be measured directly, the electronic contribution κ_e can generally be determined from the electrical conductivity by the Wiedemann–Franz law:

$$\frac{\kappa_e}{\sigma T} \approx L_0, \tag{9}$$

where the Lorenz number $L_0 = 2.45 \times 10^{-8}\,(\mathrm{V/K})^2$. Thus it is in principle straightforward to separate the electronic and lattice contributions to $\kappa(T)$. In graphite, phonons dominate the specific heat above $\sim$20 K [17], while in MWNTs and SWNTs, the phonon contribution dominates at all temperatures.

In highly crystalline materials and at high temperatures ($T > \Theta_D/10$), the dominant contribution to the inelastic phonon relaxation time τ is phonon-phonon Umklapp scattering. At low temperatures, however, Umklapp scattering disappears and inelastic phonon scattering is generally due to fixed sample boundaries or defects, yielding a constant τ. Thus at low temperature ($T < \Theta_D/10$), the temperature dependence of the phonon thermal conductivity is similar to that of the specific heat. However, in an anisotropic material, the weighting of each state by the factor $v^2\tau$ becomes important. The thermal conductivity is most sensitive to the states with the highest band velocity and scattering time. In graphite, for instance, the *ab*-plane thermal conductivity can be closely approximated by ignoring the inter-planar coupling [17]. From this argument, we would expect that the temperature-dependence of the thermal conductivity of SWNT ropes and MWNTs should be close to that of their constituent tubes. However, bundling individual tubes into ropes or MWNTs may introduce inter-tube scattering, which could perturb somewhat both the magnitude and the temperature dependence of the thermal conductivity.

2.1 Thermal Conductivity of MWNTs

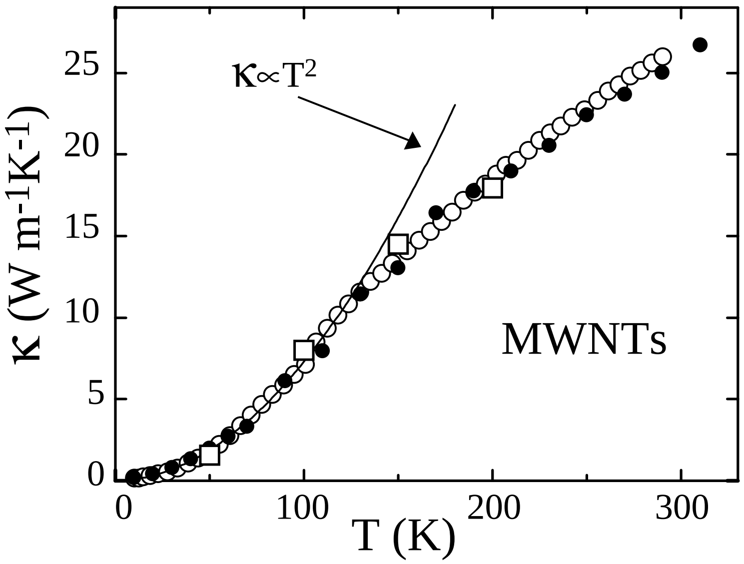

Fig. 6. Measured thermal conductivity of MWNTs [13] from 4 K to 300 K

In highly graphitic fibers, $\kappa(T)$ follows a $T^{2.3}$ temperature dependence until $\sim 100\,K$, then begins to decrease with increasing T above ~150 K [18]. This decrease in $\kappa(T)$ above 100 K is due to the onset of phonon-phonon Umklapp scattering, which grows more effective with increasing temperature as higher-energy phonons are populated. In less graphitic fibers, the magnitude of κ is significantly lower, and the Umklapp peak in $\kappa(T)$ is not seen, because grain-boundary scattering dominates $\kappa(T)$ to higher temperatures.

Figure 6 shows the thermal conductivity of CVD-grown MWNTs, on a linear scale, from 4 K to 300 K [13]. Because of the large diameter of these tubes, we expect them to act essentially as 2-D phonon materials. Indeed, at low temperature ($T < 100\,\mathrm{K}$), $\kappa(T)$ increases as $\sim T^2$, similar to the $T^{2.3}$ behavior in graphite. The room-temperature thermal conductivity is small, comparable to the less-graphitic carbon fibers, and the MWNTs do not show a maximum in $\kappa(T)$ due to Umklapp scattering; both properties are consistent with a small crystallite size.

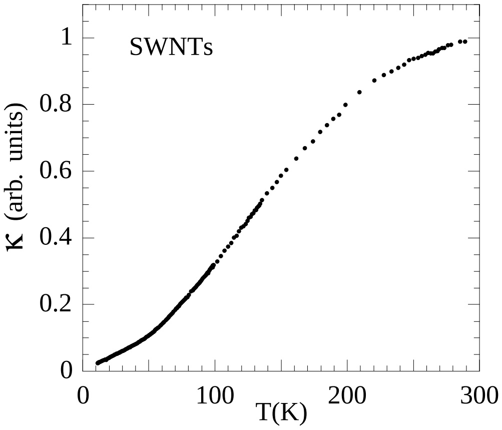

Fig. 7. Thermal conductivity of a bulk sample of SWNTs [19]

2.2 Thermal Conductivity of SWNTs

Figure 7 represents the measured $\kappa(T)$ of a bulk sample of laser-vaporization produced SWNTs, with ∼1.4-nm diameter [20]. The different temperature-dependence of $\kappa(T)$ reflects the much smaller size of SWNTs compared to MWNTs. $\kappa(T)$ increases with increasing T from 8 K to 300 K, although a gradual decrease in the slope above 250 K may indicate the onset of Umklapp scattering. Most striking is a change in slope near 35 K: below this temperature, $\kappa(T)$ is linear in T and extrapolates to zero at $T{=}0$. We will discuss the low-temperature behavior in detail below.

Although the temperature dependence of the thermal conductivity is the same for all 1.4-nm diameter SWNT samples, the magnitude of $\kappa(T)$ is sensitive to sample geometry. In disordered 'mat' samples, the the room-temperature thermal conductivity is ∼35 W/m-K. However, in samples consisting of aligned SWNTs, the room-temperature thermal conductivity is above 200 W/m-K [21], within an order of magnitude of the room-temperature thermal conductivity of highly crystalline graphite. Because even such an aligned sample contains many rope-rope junctions, it is likely that a single tube, or a rope of continuous tubes, will have significantly higher thermal conductivity than the bulk samples.

Simultaneous measurement of the electrical and thermal conductance of bulk SWNT samples yields a Lorenz ratio $\kappa/\sigma T$ which is more than two orders of magnitude greater than the value for electrons at all temperatures. Thus the thermal conductivity is dominated by phonons, as expected.

Figure 8 highlights the low-T behavior of the thermal conductivity of SWNTs [19]. As discussed above, the linear T dependence of $\kappa(T)$ likely reflects the one-dimensional band-structure of individual SWNTs, with linear acoustic bands contributing to thermal transport at the lowest temperatures and optical subbands entering at higher temperatures. $\kappa(T)$ can be modeled using a simplified two-band model (shown in the inset to Fig. 8), considering

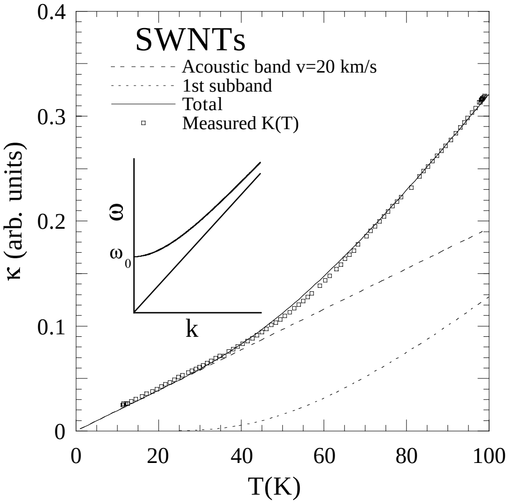

Fig. 8. Measured Low-temperature Thermal Conductivity of SWNTs, compared to a two-band model [19]

a single acoustic band and one subband. In a simple zone-folding picture, the acoustic band has a dispersion $\omega = vk$ and the first subband has dispersion $\omega^2 = v^2k^2 + \omega_0^2$, where $\omega_0 = v/R$. The thermal conductivity from each band can then be estimated using Eq. (8) and assuming a constant scattering time τ. Thus τ provides an overall scaling factor, and v sets the energy scale $\hbar\omega_0$ of the splitting between the two bands.

Figure 8 shows the measured $\kappa(T)$ of SWNTs, compared to the results of the two-band model discussed above, with v chosen to be 20 km/s, which is between that of the 'twist' ($v = 15$ km/s) and LA ($v = 24$ km/s) modes. The top dashed line represents $\kappa(T)$ of the acoustic band: it is linear in T, as expected for a 1-D phonon band with linear dispersion and constant τ. The lower dashed line represents the contribution from the optical subband; it is frozen out at low temperatures, and begins to contribute near 35 K. The solid line is the sum of the two contributions, and is quite successful in fitting the experimental data below ~100 K. The phonon energies, and temperature scale of the observed linear behavior, are higher in the thermal conductivity measurements than in the heat capacity measurements (§1.4). This may be due to the preferential weighting of higher-velocity modes in thermal conductivity, although more detailed modeling is needed to resolve this issue. The measured linear slope can be used to calculate the scattering time, or, equivalently, a scattering length. A room-temperature thermal conductivity of 200 W/m-K (as is seen in the bulk aligned samples) implies a phonon scattering length of 30 nm, although this value is likely to be higher for single tubes.

We have seen above that the small size of nanotubes causes phonon quantization which can be observed both in the heat capacity and in the thermal conductivity at low temperatures. The restricted geometry of the tubes may also affect the thermal conductivity at high temperature since Umklapp scattering should be suppressed in one dimensional system because of the unavailability of states into which to scatter [16,22]. Extension of these measurements to higher temperatures, as well as additional theoretical modeling, should prove interesting.

References

1. L. X. Benedict, S. G. Louie, and M. L. Cohen, Solid State Commun. **100**, 177–180 (1996).
2. D. Sanchez-Portal, E. Artacho, J. M. Soler, A. Rubio, and P. Ordejón, Phys. Rev. B **59**, 12678–12688 (1999).
3. R. Saito, G. Dresselhaus, and M. S. Dresselhaus, *Physical Properties of Carbon Nanotubes* (Imperial College Press, London, 1998).
4. R. Saito and H. Kataura, chapter in this volume.
5. C. Kittel, in *Introduction to Solid State Physics*, 6th ed., (John Wiley and Sons, New York, NY, 1986).
6. A. Mizel, L. X. Benedict, M. L. Cohen, S. G. Louie, A. Zettl, N. K. Budra, and W. P. Beyermann, Phys. Rev. B **60**, 3264 (1999).
7. R. Nicklow, N. Wakabayashi, and H. G. Smith, Phys. Rev. B **5**, 4951 (1972).
8. W. DeSorbo and G. E. Nichols, J. Phys. Chem. Solids **6**, 352 (1958).
9. M. G. Alexander, D. P. Goshorn, D. Guérard, P. Lagrange, M. El Makrini, and D. G. Onn, Synth. Met. **2**, 203 (1980).
10. Neil W. Ashcroft and N. David Mermin, *Solid State Physics* (Harcourt Brace College Publishers, 1976).
11. J. Hone, B. Batlogg, Z. Benes, A. T. Johnson, and J. E. Fischer, (unpublished).
12. R. Al-Jishi. *Lattice Dynamics of Graphite Intercalation Compounds.* PhD thesis, Massachusetts Institute of Technology, October 1982. Department of Physics.
13. W. Yi, L. Lu, Zhang Dian-lin, Z. W. Pan, and S. S. Xie, Phys. Rev. B Rapid Comm. **59**, R9015 (1999).
14. G. W. C. Kaye and T. H. Laby, *Tables of Physical and Chemical Constants*, 16th ed. (Longman, London, 1995).
15. R. S. Ruoff and D. C. Lorents, Carbon **33**, 925 (1995).
16. D. T. Morelli, J. Heremans, M. Sakamoto, and C. Uher, Phys. Rev. Lett. **57**, 869 (1986).
17. B. T. Kelly, in *Physics of Graphite*, (Applied Science (London), 1981).
18. J. Heremans and C. P. Beetz, Jr., Phys. Rev. B **32**, 1981 (1985).
19. J. Hone, M. Whitney, C. Piskoti, and A. Zettl, Phys. Rev. B Rapid Comm. **59**, R2514 (1999).
20. A. Thess, R. Lee, P. Nikolaev, H. Dai, P. Petit, J. Robert, C. Xu, Y. H. Lee, S. G. Kim, A. G. Rinzler, D. T. Colbert, G. E. Scuseria, D. Tománek, J. E. Fischer, and R. E. Smalley, Science **273**, 483–487 (1996).
21. J. Hone *et al.*, (unpublished).
22. R. E. Peierls, in *Quantum Theory of Solids*, (Oxford University Press, London, 1955).

Index